Mode coupling in a hanging-fiber AFM used as a rheological probe

Mode coupling in a hanging-fiber AFM used as a rheological probe

2014 EPL 106 54005

(http://iopscience.iop.org/0295-5075/106/5/54005)

A Letters Journal Exploring the Frontiers of Physics

June 2014

EPL, **106** (2014) 54005 www.epljournal.org
doi: 10.1209/0295-5075/106/54005

Mode coupling in a hanging-fiber AFM used as a rheological probe

C. Devailly, J. Laurent, A. Steinberger, L. Bellon and S. Ciliberto

Université de Lyon, Laboratoire de Physique, École Normale Supérieure de Lyon, CNRS UMR5672 46, Allée d'Italie, 69364 Lyon Cedex 07, France

received 10 November 2013; accepted in final form 14 May 2014
published online 3 June 2014

PACS 47.61.Fg – Flows in micro-electromechanical systems (MEMS) and nano-electromechanical systems (NEMS)
PACS 83.85.Jn – Viscosity measurements
PACS 05.40.-a – Fluctuation phenomena, random processes, noise, and Brownian motion

Abstract – We analyze the advantages and drawbacks of a method which measures the viscosity of liquids at microscales, using a thin glass fiber fixed on the tip of a cantilever of an ultra-low-noise Atomic Force Microscope (AFM). When the fiber is dipped into a liquid, the dissipation of the cantilever-fiber system, which is linked to the liquid viscosity, can be computed from the power spectral density of the thermal fluctuations of the cantilever deflection. The high sensitivity of the AFM allows us to show the existence and to develop a model of the coupling between the dynamics of the fiber and that of the cantilever. This model, which accurately fits the experimental data, gives also more insights into the dynamics of coupled microdevices in a viscous environment.

Introduction. – The development of the study of complex fluids needs measurements at micrometer scale to observe local properties of the media. Furthermore one often needs to measure the viscosity of very small liquid samples. For these reasons several microrheology techniques have been developed. The most common is based on the measurement of the Brownian motion properties either by tracking several free micrometer beads or by trapping them in optical tweezers [1–3]. Both techniques need a transparent fluid but an alternative method has been recently proposed in ref. [4]. This method is based on an excited suspended microchannel resonator and it works for viscosities less than $10\,\mathrm{mPa}\cdot\mathrm{s}$. In ref. [5] another technique has been proposed, which measures the thermal fluctuations of a hanging-fiber Atomic Force Microscope (AFM) probe. This method is interesting and presents several advantages with respect to the other ones: a) it can work with large viscosities; b) the fluid has not to be transparent; c) the amount of needed fluid can be very small. However the data analysis in ref. [5] relies on several assumptions that could not be checked due to the limited sensitivity of their apparatus.

In this paper we analyze the advantages and drawbacks of this method with a very-low-noise AFM. This improved sensitivity allows us to measure relatively high viscosities and most importantly to develop a model for the fiber-fluid interaction, which is more appropriate and precise than that of ref. [5]. Thus the results of this paper are not only useful for microrheology measurements of rather viscous and opaque fluids but also to investigate the basic dissipation mechanisms of a thin fiber inside a fluid and to give more insights into the mechanical coupling of such microdevices.

Experimental set-up. – The measurement of the fluid viscosity is performed using a cylindrical micro-rod fixed to an AFM cantilever, as sketched in fig. 1. The rod is immersed into the fluid whose friction along its length produces an extra damping for the cantilever, which is detected by measuring the thermal noise of the cantilever.

The rod is fabricated using an optical single-mode fiber, stretched under the flame of a blowtorch: its initial $125\,\mu\mathrm{m}$ diameter is thinned to $d \approx 3\,\mu\mathrm{m}$. The fiber is glued at the apex of an AFM cantilever with a two-components epoxy adhesive (Araldite). We use standard AFM cantilevers (Budget Sensors AIO): soft ones with a stiffness $k_c \approx 0.25\,\mathrm{N/m}$ and a resonance frequency $f_0 \approx 8\,\mathrm{kHz}$, and stiffer ones with $k_c \approx 4\,\mathrm{N/m}$ and $f_0 \approx 60\,\mathrm{kHz}$ (resonant frequencies after functionalization of the tip). A particular effort is done to glue the fiber as perpendicular to the cantilever as possible to avoid torsion modes. The fiber is cut at the appropriate length (around $200\,\mu\mathrm{m}$) using a sharp tweezer and a diamond tool. These operations are performed under a bright light microscope with a $\times 20$ magnification, using micromanipulators (from Narishige). Finally the probes characteristics are checked with the

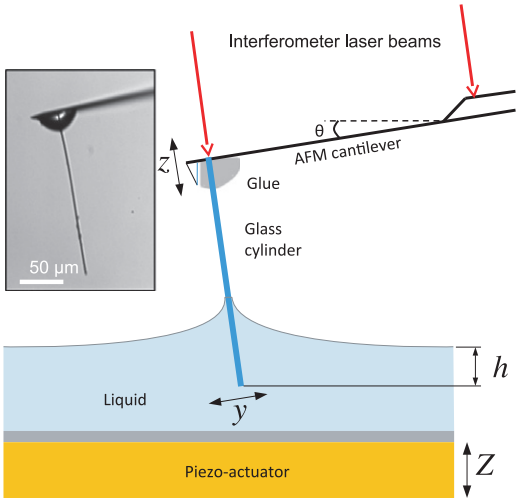

Fig. 1: (Colour on-line) Experimental set-up. The fiber glued to the cantilever is dipped in a liquid layer on a depth h, controlled by the position Z of the piezo-actuator. The two laser beams of the interferometer measure the cantilever deflection z. The fiber deflection is noted y. The picture on the left is an image of the fiber taken with a bright field microscope $\times 10$ magnification.

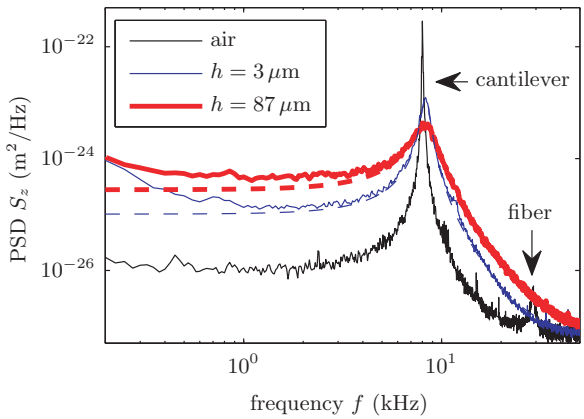

Fig. 2: (Colour on-line) Soft cantilever, hexadecane. Solid line: measured PSD $S_z^{\rm meas}$ for several dipping depths h. Dashed line: fit with the spectrum $S_{z,0}^{\rm SHO}$ of the SHO model using only the data around the resonance (see text for details).

microscope images (fig. 1) and we use only those in which the fiber-cantilever angle is within the range [85°, 95°].

The hanging-fiber probe is mounted on a home-built atomic force microscope. The deflection z of the cantilever (fig. 1) is measured by an interferometric deflection sensor [6], inspired by the original design of Schonenberger [7] with a quadrature phase detection technique [8]: the interference between the reference laser beam reflecting on the static base and the sensing beam on the tip of the cantilever gives a direct measurement of the deflection with a very high accuracy (see spectra fig. 2). This technique offers a very low intrinsic noise (down to $10^{-14}\,\mathrm{m}/\sqrt{\mathrm{Hz}}$ [6]) and it is intrinsically calibrated. Thanks to this high resolution, no external excitation of the cantilever is required, and its thermal fluctuations can be measured over a wide frequency range.

The viscosity measurement is performed using the same fiber with 4 different liquids: alcanes (dodecane and hexadecane) and silicone oils (of viscosity $10\,\mathrm{mPa\cdot s}$ and $20\,\mathrm{mPa\cdot s}$, respectively denoted 10v and 20v) chosen for their range of viscosity, their weak evaporation, and their good wetting of the glass fiber. The liquid is put in a 1.4 cm diameter copper container placed under the fiber; the liquid layer is about 1 mm deep. When changing the liquid, the fiber is rinsed thoroughly with the new liquid, and the copper container is rinsed as well before putting fresh liquid in it. Silicone oils have been studied after alcanes, in an increasing order of viscosity. The pool can be moved along the vertical axis Z by a piezo-actuator. The measurements are performed at 25 °C.

In order to change the vertical height h between the tip of the fiber and the undisturbed surface of the liquid (see fig. 1), the position Z of the container is changed in $3\,\mu$m steps. We wait a few seconds after the displacement before starting the measurement to let the fluid relax. The origin of the height h is located with a $3\,\mu$m uncertainty either from the jump of the static deflection due to the capillary force on the fiber or from the sudden broadening of the noise spectra between two displacement steps. The error on the relative height results from the mechanical drift of the actuator and the evaporation of the liquid, and is estimated to be lower than $5\,\mu$m for a typical $100\,\mu$m dipping experiment. By making several approach-separation cycles we checked that the meniscus height is less than $12\,\mu$m and that the wetting layer has a negligible effect on the results.

The cantilever deflection is sampled for at least 5 s, with a 24 bits resolution, at 240 kHz for the soft cantilever and 500 kHz for the stiff one. The Power Spectral Density (PSD) of the deflection is calculated with a resolution of about 100 Hz for the data in liquid and 25 Hz for data in air. The spectra are averaged more than 1000 times in order to reduce the statistical noise.

Data analysis and parameters definition. – In figs. 2 and 3 the measured PSD $S_z^{\rm meas}$ of the cantilever deflection induced by the thermal noise is plotted at several dipping depth h in hexadecane for the soft and stiff cantilevers. The broadening of the resonance peak shows the increase of damping as a function of h.

In order to check the quality of the measurement and to extract a reliable value of the viscosity one has to fit the PSD in a wide frequency range. As there is no external force acting on the system, we can use the Fluctuation Dissipation Theorem (FDT) [9], linking the mechanical response function of the total system to the PSD $S_z(f)$ of the cantilever deflection z:

$$S_z(f) = -\frac{4k_{\rm B}T}{\omega}\mathrm{Im}\left(\frac{1}{G(\omega)}\right) = \frac{4k_{\rm B}TG''}{\omega|G|^2}, \qquad (1)$$

where $G = G' + iG''$ is the the inverse of the mechanical response function of the total system, $k_{\rm B}$ is the Boltzmann

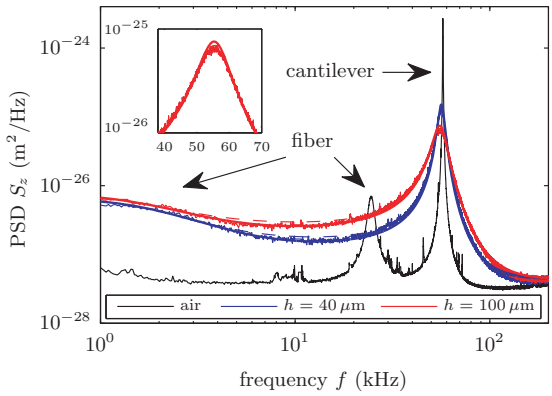

Fig. 3: (Colour on-line) Stiff cantilever, hexadecane. Solid line: measured PSD $S_z^{\rm meas}$ for several dipping depths h. Dashed line: fit with $S_{z,0}^{\rm CHO}$. Bold solid line: fit with $S_{z,B}^{\rm CHO}$. Black: air, blue: $h = 40\,\mu$m, red: $h = 100\,\mu$m.

constant, T the temperature, Im(.) stands for the imaginary part and $\omega = 2\pi f$ is the angular frequency. For a Simple Harmonic Oscillator (SHO) with viscous damping for example, the response function is [9]:

$$G(\omega) = k - m\omega^2 + i\gamma\omega \tag{2}$$

with k, m and γ respectively the stiffness, mass and damping coefficient of the SHO.

A model for the damping. The key point is to have a reliable model for G and most importantly of the damping coefficient of this system, assuming that the fiber is a cylinder oscillating along its axis. As far as we know there are no exact analytical solutions to this problem and one has to do several approximations. The starting point is the Stokes' solution for the drag of a sphere oscillating at frequency ω in a fluid of viscosity η and density ρ [10]. Supposing that there are only geometric corrections for the fiber we can write the dissipation γ_c of the fiber-cantilever system as

$$\gamma_c = \gamma_0(h,d) + b\sqrt{2}\frac{d}{\delta}\eta h = \gamma_0(h,d) + bd\sqrt{\rho\eta\omega}\,h, \tag{3}$$

where $\delta = \sqrt{2\eta/(\rho\omega)}$ is the viscous penetration length and b a generic geometric factor to be determined ($b = b(h,d)$ may depend on the values of h and d). An approximated solution for the viscous coefficient γ_0 for a fully immersed rod is [11]:

$$\gamma_0(h,d) = \gamma_\odot + \frac{2\pi}{\ln(h/d) + \epsilon}\eta h, \tag{4}$$

where the constant $\gamma_\odot$ is the sum of the dissipation in the liquid meniscus and of the effective dissipation of the cantilever in air. The coefficient ϵ is a correction (smaller than 1), which depends on the shape of the fiber's cross-section[1]. Except for the correction in $\ln(h/d)$, γ_0 has a leading linear behavior in our range of h. As pointed out in ref. [10] the term in $\sqrt{\omega}$ in eq. (3) becomes relevant only if $d > \delta$, thus it can be usually neglected at low frequencies. Using eq. (3), we can compute [10] the storage modulus G' and the loss modulus G'' of the fiber-cantilever system:

$$G'(\omega) = k_c + k_m - (m_c + m_{\rm fluid})\omega^2 - bd\sqrt{\eta\rho}\,\omega^{3/2}\,h, \tag{5}$$

$$G''(\omega) = \gamma_0\omega + bd\sqrt{\eta\rho}\,\omega^{3/2}\,h, \tag{6}$$

where k_c is the stiffness of the cantilever, k_m is the meniscus stiffness, m_c is the effective mass of the cantilever-fiber system, and $m_{\rm fluid}$ is the mass of the displaced fluid. In our case, $m_{\rm fluid}$ represents in the worst case of a totally immersed fiber only 3% of m_c and it will be neglected. k_m is of the order of magnitude of the liquid's surface tension, a few tens of mN/m; we will not consider its possible frequency dependence in this work. Inserting expressions (5) and (6) in eq. (1) we get

$$S_z = \frac{4k_{\rm B}T(\gamma_0 + \tilde{B}\sqrt{\omega}\,h)}{(k - m_c\omega^2 - \tilde{B}\omega^{3/2}\,h)^2 + (\gamma_0\omega + \tilde{B}\omega^{3/2}\,h)^2} \tag{7}$$

with $k = k_c + k_m$ and $\tilde{B} = bd\sqrt{\eta\rho}$. Note that this way we consider the cantilever-fiber system as a SHO with a frequency-dependent damping coefficient γ_c and a frequency-dependent added mass that can be viewed as the mass of fluid in the boundary layer.

This model, which takes into account the effect of the boundary layer to compute dissipation, will be noted model SHO$_B$ and the predicted spectrum $S_{z,B}^{\rm SHO}(f)$ where four free parameters have to be adjusted to fit the data: k, m_c, γ_0 and $\tilde{B}$. However when the resonance frequency is small enough (*i.e.* $d < \delta$) then we may impose $\tilde{B} = 0$. In this case, we recover the classic SHO model, noted SHO$_0$, leading to the spectrum $S_{z,0}^{\rm SHO}(f)$.

Simple Harmonic Oscillator. We consider first the SHO model for the soft cantilever. Indeed at the resonance frequency (8.2 kHz), δ varies between 6.8 μm for dodecane and 28 μm for silicone oil 20v, thus for all the liquids that we use $\delta > d \simeq 3\,\mu$m and $\tilde{B}$ can be neglected. We therefore fit the spectra using $S_{z,0}^{\rm SHO}(f)$ which has the advantage of having only three free parameters.

In order to measure γ_0 we proceed in the following way. To begin with, we simply fit the resonant frequency peak, as done in ref. [5], for each dipping depth h and each liquid. This method is not very precise because the values of γ_0 depend on the chosen fitting range around the soft resonance. Therefore, one has to decide a criterium to select this fitting range, which, in our case, is chosen in order to have the best fit in the largest part of the spectra. The results of these fits around the resonance peak are shown in fig. 2. We notice that the spectra $S_{z,0}^{\rm SHO}$ do not fit properly our data at low frequency where some extra noise is present below 2 kHz. The use of one more free parameter with model SHO$_B$ does not improve the quality of the fitting, because the additional terms deform the SHO$_B$ noise spectrum even further away from our data.

[1] In the ellipsoid model described in ref. [11] and used by Xiong *et al.* [5], ϵ does not depend on h in our h/d range and is equal to 0.19. In a cylinder approximation [11], ϵ varies between -0.55 and -0.58 and eq. (4) is valid only for a ratio $h/d > 4$.

In order to understand where the noise increase at $f < 2\,\mathrm{kHz}$ is coming from, we analyze more precisely the spectra in fig. 2. We notice that the spectrum in air presents another resonance at about 29 kHz, which corresponds to the first flexion mode of the fiber oscillations. This resonance disappears when the fiber is immersed. To find out what happens to this resonance, we decided to do the same measurement with the same kind of fiber (length and diameter) on a more rigid cantilever having a resonance around 60 kHz. The aim is to avoid damping the fiber noise in the inertial tail of the resonance. The spectra measured in air and in hexadecane using this stiffer cantilever-fiber system are plotted in fig. 3. In the spectrum in air, we clearly see the resonance of the cantilever at 57 kHz and the resonance of the fiber at 24 kHz, at approximately the same frequency than the previous system. When the fiber is dipped into the fluid this resonance becomes over-damped and the cut-off frequency goes towards low frequencies close to 2 kHz. In contrast, the resonance of the stiff cantilever behaves similarly to that of the soft one, presenting a continuous broadening of the resonance peak as a function of h. All these remarks suggest that there is probably a coupling between the fiber and the cantilever oscillations which perturbs the simple picture of a SHO.

Coupled oscillators. Let us develop a model of Coupled Harmonic Oscillators (CHO) for the cantilever (deflection z) and the fiber (deflection y of its extremity). In a first approximation, the cantilever motion corresponds to a forcing of the clamping base of the fiber along its axis, thus we will neglect the effect of the cantilever deflection on that of the fiber. The fiber is thus modeled as a classic SHO and the Fourier transform y_ω of its deflection y is described by

$$(k_f - m_f\omega^2 + i\gamma_f\omega)y_\omega = F_f, \tag{8}$$

where m_f, γ_f and k_f are, respectively, the effective mass, dissipation and stiffness of the fiber and F_f is a delta-correlated thermal noise acting on the fiber, whose spectrum is $S_{F_f} = 4k_\mathrm{B}T\gamma_f$. The PSD of the fiber thermal noise is

$$S_y(f) = \frac{4k_\mathrm{B}T\tau_f}{k_f[(1-\omega^2/{\omega_f}^2)^2 + (\tau_f\omega)^2]}, \tag{9}$$

where $\omega_f = \sqrt{k_f/m_f}$ is the resonance of the fiber and $\tau_f = \gamma_f/k_f$ is the fiber relaxation time.

The fiber motion applies a torque on the cantilever end, thus the equation describing the Fourier transform z_ω of z is coupled to the fiber deformation y:

$$(G' + iG'')z_\omega = F_c + \alpha y_\omega, \tag{10}$$

where G' and G'' are defined in eqs. (5) and (6), and F_c is a delta-correlated thermal noise, whose spectrum is $S_{F_c} = 4k_\mathrm{B}T\gamma_c$. The term αy (with α the coupling coefficient) assumes the simplest coupling with the deflection of the fiber y. The PSD $S_z^{\mathrm{CHO}}(f)$ of z can be computed from eqs. (8) and (10) by making the very reasonable hypothesis that F_f and F_c are uncorrelated noise. We get

$$S_{z,n}^{\mathrm{CHO}}(f) = S_{z,n}^{\mathrm{SHO}}(f) + \frac{\alpha^2}{|G|^2}S_y(f), \tag{11}$$

where n stands for either 0 or B depending whether we impose $\tilde{B} = 0$ or not.

When the fiber is dipped into the fluid, we notice that the motion of the fiber is over-damped, *i.e.* $\tau_f \gg 1/\omega_f$. Thus eq. (9) reduce to a Lorentzian where $(1-\omega^2/{\omega_f}^2)^2 = 1$. We can try to fit our data with these CHO_n models, *i.e.* eqs. (11) and (9). Because of the large number of parameters in the model we proceed in the following way using first the model CHO_0 with $\tilde{B} = 0$. We begin to fit the spectrum around the cantilever resonance to estimate γ_0 and to obtain a first approximation of $S_{z,0}^{\mathrm{SHO}}$. Inserting this first approximation in eq. (11), we can fit the expression $S_z^{\mathrm{meas}}/S_{z,0}^{\mathrm{SHO}} - 1$ with a Lorentzian, from which the values of k_f/α^2 and τ_f are obtained. Using these values in eq. (11) one can improve the fit of $S_{z,0}^{\mathrm{SHO}}$ and repeat the iteration. After 3 iterations the values of the parameters become stable and we obtain a good fit on the whole frequency range (fig. 3). The $S_{z,0}^{\mathrm{CHO}}$ fits well the resonant peak as can be seen in the inset of fig. 3. However we see that the fit is not correct around 10 kHz where the fitting curve is systematically above the data. The problem could come from the fact that we perform the fit around the resonance at 60 kHz keeping $\tilde{B} = 0$. At such a high frequency the CHO_0 model is probably not adequate because the boundary layer thickness δ is about $4.5\,\mu\mathrm{m}$, which is close to the fiber diameter. Thus one should use the CHO_B model which takes into account the boundary layer effects.

To fit the data with $S_{z,B}^{\mathrm{CHO}}(f)$, we use the same iteration approach with one difference: to reduce the number of free parameters, the stiffness and mass are now fixed to the values measured in air, $k_c^{\mathrm{air}} = 3.7\,\mathrm{N/m}$ and $m_c^{\mathrm{air}} = 2.9 \times 10^{-11}\,\mathrm{kg}$. This is justified because the other contributions to the stiffness and mass are negligible with respect to the values in air in the high frequency experiment. After several iterations we get a correct fit of the data except around the resonance (see the inset of fig. 3) where the fit $S_{z,B}^{\mathrm{CHO}}(f)$ is higher than the data. This indicates that this model for the cantilever's resonance at high frequency is not perfect. Thus we conclude that in order to discriminate between the two models ($\tilde{B} = 0$ and $\tilde{B} \neq 0$), we would need an even larger frequency range. One could check at low frequencies, where $S_{z,B}^{\mathrm{SHO}}(f)$ has a dependence in $\sqrt{\omega}$ instead of the flat curve of $S_{z,0}^{\mathrm{SHO}}(f)$. But in our data, the low-frequency part is hidden by $S_y(f)$. On the other hand, one could use the high-frequency part of the spectra. Indeed at high frequency, $S_{z,B}^{\mathrm{CHO}}(f)$ should decrease in $\omega^{-7/2}$ instead of ω^{-4} of $S_{z,0}^{\mathrm{SHO}}(f)$. But in this case the intrinsic noise of the interferometer hides the data and this comparison is not possible. Besides, we could see in air the second mode of the fiber very close to the

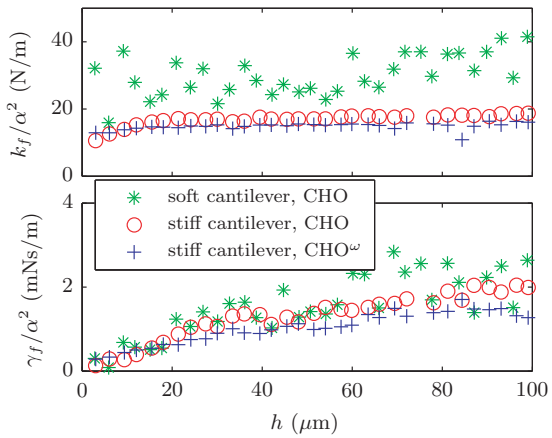

Fig. 4: (Colour on-line) Evolution of the fiber stiffness k_f and damping coefficient γ_f as a function of the dipping depth h of the fiber in hexadecane. The stiffness is constant, while the damping increases from 0 and saturates for large h, where immersion approaches the base of the fiber.

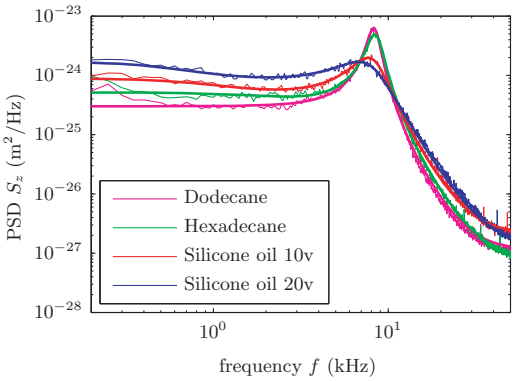

Fig. 5: (Colour on-line) Soft cantilever, dipping depth about 63 μm: PSD $S_z^{\mathrm{meas}}(f)$ of the measured thermal noise for each liquid (thin lines); fit with $S_{z,0}^{\mathrm{CHO}}(f)$, modeling the coupled oscillators (thick lines).

cantilever's resonance on most high-frequency probes we tested, so that this mode may also disturb the cantilever's resonance. As a result, it is not possible to clearly separate the two contributions to the dissipation γ_c from our measured noise spectra.

We can see in fig. 4 the evolution of the stiffness k_f and the dissipation γ_f of the fiber lateral oscillations as a function of dipping depth estimated from the two models. It is interesting to notice that the values obtained from the two models are very close and have a dependence on h which is quite reasonable. Except at the very beginning[2], the stiffness is constant as expected. Instead, the dissipation increases and tends to saturate at large h. This behavior can be understood considering that γ_f is the damping of the deflection mode of the fiber which has a large displacement at the free extremity and a small one towards the anchoring point. Therefore the non moving part of the

[2]When the fiber is just touching the liquid, surface tension effects may perturb the measurement.

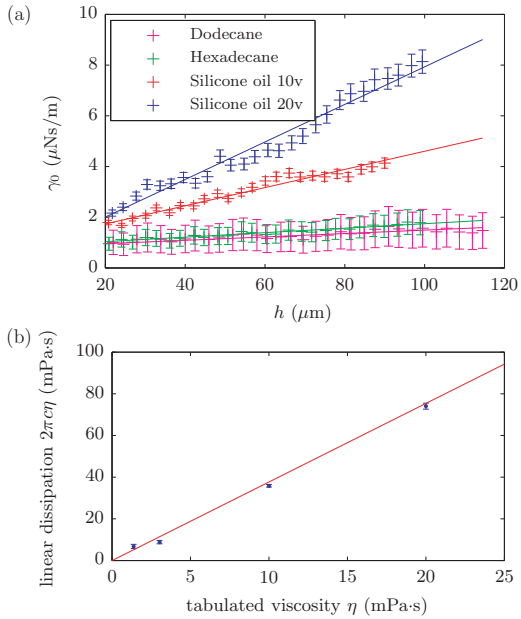

Fig. 6: (Colour on-line) (a) Dissipation γ_0 as a function of h for each liquid. (b) Linear dissipation of each liquid ($2\pi c\eta$) as a function of the tabulated viscosity for alcanes and silicone oils.

fiber will not contribute to dissipation and γ_f increases fast at small h (region of large lateral displacement) and saturates above a certain h (region of small displacement). From this data it is possible to have the order of magnitude of α. Indeed taking into account the size of the fiber and its Young modulus one estimates $k_f \simeq 0.1\,\mathrm{N/m}$ and $\alpha \simeq 0.06$–0.07 which is a reasonable value for the coupling.

Looking at fig. 2 we notice that the resonance of the fiber in air is about at the same frequency for the soft probe as for the stiffer one[3]. We can thus suppose that the cut-off frequency when the fiber is immersed is also around 2 kHz, that is to say, at the left of the cantilever resonance. Therefore we can use the same iteration than before to analyze our spectra using eq. (9) for the spectrum of the fiber and model CHO_0. In fig. 5, we can see fits for each liquid at $h = 63\,\mu$m. We see that now the model fits our data properly on the whole frequency range. We can also see in fig. 4 the same evolution for the stiffness and the dissipation of the fiber. Data are noisier than those at high frequency because the resonance of the cantilever is closer to the cut-off frequency of the fiber.

Viscosity measurement at low frequency. In order to perform viscosity measurements, we choose to focus on low-frequency measurements, which present several benefits when compared to high-frequency measurements. Firstly the hanging-fiber probes are less difficult to fabricate on softer and longer cantilevers. Secondly, the signal over noise ratio is much higher with soft cantilevers. Finally, the viscosity measurement is based on

[3]In fig. 2 the amplitude of the fiber resonance is very low because being at a frequency larger than the cantilever resonance, it is strongly filtered by the cantilever response (see eq. (11)).

the dissipation γ_0, and requires neither the calibration of the unknown coefficient b not the knowledge of the liquid's density ρ.

We extract the dissipation coefficient γ_0 for each liquid at each depth from the CHO_0 fitting procedure on the soft probe's data. The results are plotted in fig. 6(a), where we can see a linear behavior as a function of h in the displayed immersion range where $h/d > 6$. The error bars take into account the standard deviation of the mass and the stiffness of the cantilever during the dipping. Our range in h is too small to measure the logarithmic correction of eq. (4) and we rewrite it as: $\gamma_0 = \gamma_\odot + 2\pi c\eta h$, where c is a parameter that depends on the geometry of the probe. From the plot of fig. 6(a), we extract the slope $2\pi c\eta$ for each liquid, and plot it in fig. 6(b) as a function of the tabulated viscosity η. The data are aligned on a straight line which correctly crosses the (0,0) point with a slope $2\pi c = 3.67 \pm 0.07$. We thus obtain $c = 0.58 \pm 0.01$.

This value is interesting because it clearly excludes that γ_0 is simply given by eq. (4). Indeed for our measuring range $6 < h/d < 30$ and for $-1 < \epsilon < 0$ one finds that the function $h/(\ln(h/d)+\epsilon)$ is well approximated by a straight line $(c'h + c'_o)$ with c' always very close to 0.2, which is incompatible to the measured value of c. This difference is not so surprising since the model in ref. [11] considers a fully immersed fiber whereas it crosses the liquid-air interface in our system, and a small transverse component in the driving by the cantilever also contributes to the measured dissipation. Thus it is necessary to calibrate c for each fiber using reference fluids to have reliable results.

Conclusion. – In this paper, we have analyzed the method of ref. [5] for the measurement of the local viscosity at micrometer scales. This method has several advantages, but it must be used with some precautions. Indeed, the high sensitivity of our apparatus allows us to show the existence of a fiber-cantilever coupling which may strongly perturb the measure. We propose a model which takes into account this coupling and fits the thermal noise spectra. Of course the effect of the coupling can be tuned. For example, by increasing the resonant frequency of the cantilever, we can clearly separate the frequency of the first mode of the cantilever and the first mode of the fiber. This increases the quality of the data for the fiber's mode but does not simplify the viscosity measurements from the cantilever's resonance. We have tested a model taking into account the frequency-dependent boundary layer terms (model SHO_B), but could not discriminate it from a simpler SHO_0 model by fitting the measured spectra, despite our high-resolution deflection sensor. As a result, we prefer using the simpler model with less free parameters.

Taking into account the coupling, with our low-noise AFM, we can measure the viscosity between $1\,\mathrm{mPa\cdot s}$ and at least $20\,\mathrm{mPa\cdot s}$, with 5% of accuracy for its absolute value. The accessible viscosity range is limited at $1\,\mathrm{mPa\cdot s}$ in our measurements because for lower viscosities the fiber's mode becomes too close to the cantilever's mode and cannot be separated from it. The upper viscosity bound has not been reached yet, since over-damped motion for higher viscosities can still be analyzed. In our analysis we assume a no-slip boundary condition on the fiber, which is justified because the intrinsic slip length remains below 30 nm for simple liquids [12] (while it reaches the micrometric scale for polymer melts [13]). Beware that boundary slippage can strongly affect the b and c coefficients when working with nano-fibers like in refs. [14,15] or when studying polymer melts with micro-fibers as in [16].

Finally our analysis on the cantilever fiber-coupling shows that using functionalized cantilevers is often a good idea but it is necessary to check the influence of added elements [17]. In general our results give more insights into the dynamics of coupled microdevices in a viscous environment.

* * *

This paper has been supported by the ERC project OUTEFLUCOP.

REFERENCES

[1] Squires T. M. and Mason T. G., *Annu. Rev. Fluid Mech.*, **42** (2010) 413.

[2] Gittes F., Schnurr B., Olmsted P. D., MacKintosh F. C. and Schmidt C. F., *Phys. Rev. Lett.*, **79** (1997) 3286.

[3] Gomez-Solano J. R., Petrosyan A. and Ciliberto S., *EPL*, **98** (2012) 10007.

[4] Lee I., Park K. and Lee J., *Rev. Sci. Instrum.*, **83** (2012) 116106.

[5] Xiong X., Guo S., Xu Z., Sheng P. and Tong P., *Phys. Rev. E*, **80** (2009) 061604.

[6] Paolino P., Aguilar Sandoval F. and Bellon L., *Rev. Sci. Instrum.*, **84** (2013) 095001.

[7] Schonenberg C. and Alvarado S. F., *Rev. Sci. Instrum.*, **60** (1989) 3131.

[8] Bellon L., Ciliberto S., Boubaker H. and Guyon L., *Opt. Commun.*, **207** (2002) 49.

[9] de Groot S. R. and Mazur P., *Non Equilibrium Thermodynamics* (Dover) 1984.

[10] Landau L. D. and Lifshitz E. M., *Fluid Mechanics* (Pergamon Press, London) 1966.

[11] Brorsma S., *J. Chem. Phys.*, **32** (1960) 1632.

[12] Bouzigues C. I., Bocquet L., Charlaix E., Cottin-Bizonne C., Cross B., Joly L., Steinberger A., Ybert C. and Tabeling P., *Philos. Trans. R. Soc. A*, **366** (2008) 1455.

[13] Léger L., Hervet H., Massey G. and Durliat E., *J. Phys.: Condens. Matter*, **9** (1997) 7719.

[14] Delmas M., Monthioux M. and Ondarçuhu T., *Phys. Rev. Lett.*, **106** (2011) 136102.

[15] Yazdanpanah M. M., Hosseini M., Pabba S., Berry S. M., Dobrokhotov V. V., Safir A., Keynton R. S. and Cohn R. W., *Langmuir*, **24** (2008) 13753.

[16] Sauer B. B. and Kampert W. G., *Colloid Interface*, **199** (1998) 28.

[17] Laurent J., Steinberger A. and Bellon L., *Nanotechnology*, **24** (2013) 225504.